New Astronomy 121 (2025) 102435

Contents lists available at ScienceDirect

New Astronomy

journal homepage: www.elsevier.com/locate/newast

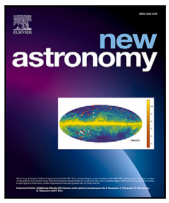

Detection of CRSF in Cep X-4 at a low luminosity level

Kinjal Roy [a,*], Rahul Sharma [a,b]

[a] Raman Research Institute, C. V. Raman Avenue, Bengaluru, 560080, Karnataka, India
[b] Inter-University Centre for Astronomy and Astrophysics, Ganeshkhind, 411007, Maharashtra, India

ARTICLE INFO

Keywords:
Accretion
X-rays
Individual
Cepheus X-4

ABSTRACT

The BeXRP *Cep X-4* underwent a type II outburst during July 2023, during which *NuSTAR* made two observations of the source. In this paper, we present the spectral and timing analysis of *Cep X-4* during this outburst. Pulsations were detected from the source at the neutron star spin period of ∼ 66 s from both observations. We detected a CRSF feature at an energy of $27.3^{+1.5}_{-1.0}$ keV in the spectrum of *Cep X-4* during the first observation. In the second observation conducted a day later when the source luminosity dropped by a factor of five, no CRSF could be detected significantly. A positive correlation between CRSF energy and luminosity was observed using data from multiple outbursts since 1998. The collisionless shock model provides a good fit to the observed variations of cyclotron line energy with luminosity, giving a surface magnetic field strength of $\sim 2.6\times 10^{12}$ G.

1. Introduction

Transient X-ray binary pulsars with Be-type main sequence companion (BeXRP) are uniquely suited to test accretion onto highly magnetized neutron stars (NSs). The BeXRPs are known to exhibit a wide range of luminosity, ranging from 10^{37-38} erg s^{-1} during the peak of outbursts to 10^{32-34} erg s^{-1} during the quiescence phase (Tsygankov et al., 2017). Many BeXRPs have been detected since the launch of the first X-ray telescopes, however, development of highly-sensitive X-ray instruments like *Chandra*, *NuSTAR* and *XMM*-Newton allow us to study the BeXRPs at much lower luminosities across a wide range of energy (Tsygankov et al., 2017; Raman et al., 2023).

In highly magnetized (B $\geq$ 10^{12} G) NSs that are part of binary systems, the accreted matter gets channeled along the magnetic field lines to the poles of the NS. The presence of strong magnetic fields at the polar regions leads to the quantization of electron energy levels (E_n in keV) in accordance to the Landau levels (Meszaros, 1992)

$$E_n = \frac{n}{1+z} \times \frac{eB\hbar}{m_e c} \sim \frac{11.6 \times n \times B_{12}}{1+z} \text{keV} \quad (1)$$

where m_e is the mass of an electron, B_{12} is the magnetic field strength in units of 10^{12} G and $n = 1, 2, 3, 4, ..$ denote the different energy levels. Cyclotron Resonant Scattering Feature (CRSF) is the absorption feature in the spectra of pulsars due to interactions between photons and electrons in quantized energy levels present in the line forming region of the NS. This spectral feature facilitates the direct measurement of the magnetic field strength of NS. Out of more than two hundred and fifty known NSs in binaries around only fifty sources show CRSF.[1] It is not clear why certain NS show CRSF while others do not. The CRSF parameters are known to show variable behavior with source luminosity (Staubert et al., 2019, and references therein). The study of cyclotron line variation with luminosity provide an excellent diagnostic tool for the study of accretion mechanisms in highly magnetized NSs.

The transient BeXRP *Cepheus X-4* (henceforth *Cep X-4*) was discovered in 1972 by *OSO−7* (Ulmer et al., 1973). Since discovery, the source has undergone multiple outbursts in 1988 (Roche et al., 1997), 1993 (Makino and GINGA Team, 1988), 2002 (McBride et al., 2007), 2012 (Fürst et al., 2015), 2014 (Vybornov et al., 2017), 2018 (Mukerjee and Antia, 2021). The spin period of *Cep X-4* is ∼ 66 s (Koyama et al., 1991). The distance to the source was estimated to be 7.4±0.5 kpc from *GAIA* DR3 data (Bailer-Jones et al., 2021; Gaia Collaboration et al., 2023).

A CRSF was first detected in the spectrum of *Cep X-4* at 30.5 ± 0.4 keV during the 1988 outburst of the source using *GINGA* telescope (Mihara et al., 1991). The CRSF was later confirmed during the 2002 outburst with *RXTE* data (McBride et al., 2007). Detailed study of the CRSF using *NuSTAR* data during the 2014 outburst, showed a clear asymmetry in the CRSF profile with an additional CRSF at around 19 keV (Fürst et al., 2015; Bhargava et al., 2019). Later, the same *NuSTAR* data was used to detect the first harmonic of the 30 keV CRSF at ∼ 55 keV (Vybornov et al., 2017). A positive correlation between the CRSF line center and X-ray luminosity from pulse amplitude resolved

* Corresponding author.
E-mail address: kinjal@rrimail.rri.res.in (K. Roy).

[1] http://orma.iasfbo.inaf.it:7007/~mauro/pulsar_list.html

https://doi.org/10.1016/j.newast.2025.102435
Received 10 January 2025; Received in revised form 12 April 2025; Accepted 26 May 2025
Available online 13 June 2025

Table 1
Observation details of the two *NuSTAR* observations.

Observation ID	Date	MJD	Exposure
90901322002	7 July 2023	60 132	26 ks
90901322004	8 July 2023	60 133	31 ks

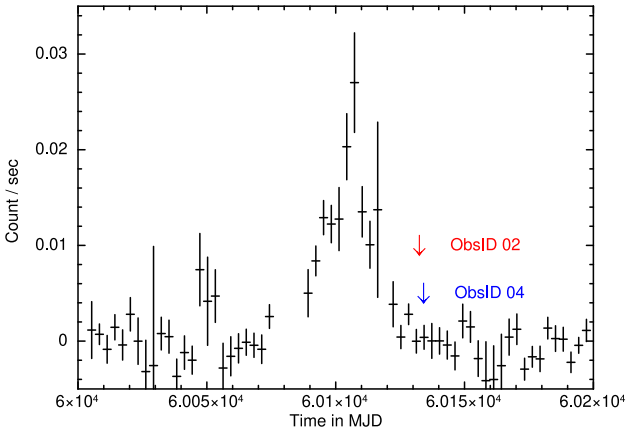

Fig. 1. The *Swift*/BAT light curve from *Cep X-4* with a binning of 3 days is shown in black. The red and blue arrows correspond to the two *NuSTAR* observations of the source from 7 July 2023 and 8 July 2023, respectively.

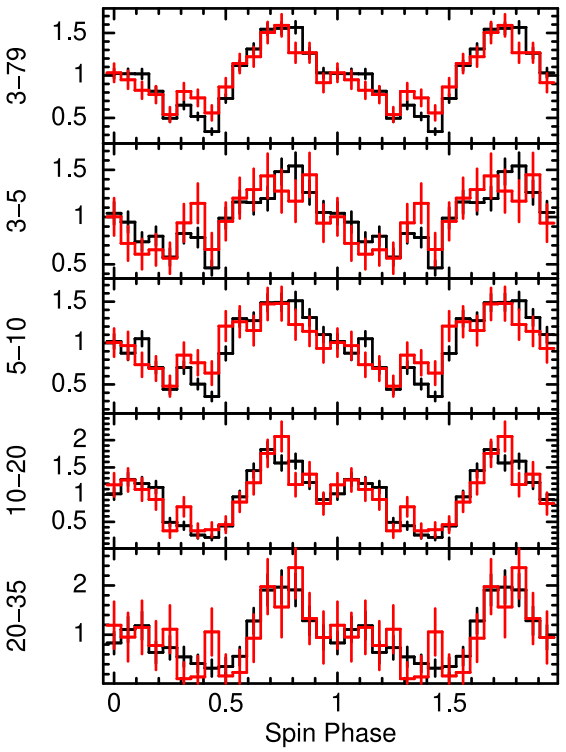

Fig. 2. The pulse profile of the source for ObsID 02 (in black) and ObsID 04 (in red). The top panel consists of the pulse profile in the energy range of 3–79 keV. The remaining panels from the top show the energy-resolved profiles in the energy ranges of 3–5, 5–10, 10–20, and 20–35 keV keV, respectively.

analysis was found (Vybornov et al., 2017). Combining all previous data along with the *Astrosat* observation of *Cep X-4* during its 2018 outburst, Mukerjee and Antia (2021) showed that the CRSF central energy remained stable at an average value of 30.2 ± 0.2 keV across a span of about thirty years.

Cep X-4 underwent a type II outburst in June 2023, which was detected by *MAXI*/GSC, *Swift*/BAT and *Fermi*/GBM (Nakajima et al., 2023). Two observations were made by Nuclear Spectroscopic Telescopic ARray (*NuSTAR*) during the decay phase of the outburst. Here, we report on the detection of CRSF in *Cep X-4* at the lowest luminosity level. We also study the evolution of CRSF with the luminosity of NS using all confirmed detections of CRSF from the source.

2. Instruments, observation and data reduction

NuSTAR is a broadband X-ray imaging and spectroscopic mission. *NuSTAR* has hard X-ray focusing optics with two identical co-aligned focal plane modules (FPM), namely FPMA and FPMB (Harrison et al., 2013). *NuSTAR* has a broadband 3–79 keV energy range with a spectral resolution of 400 eV at 10 keV. *NuSTAR* made two observations of *Cep X-4* on 7 July and 8 July 2023, details of which are given in Table 1.

The long-term *Swift*/BAT lightcurve in the 15–50 keV energy range from *Cep X-4* binned to 3 days interval is shown in Fig. 1. The *NuSTAR* observation was taken towards the end of an outburst and are marked with arrows in Fig. 1.

The *NuSTAR* data was reduced using `HEASOFT` v 6.30.1 along with the latest calibration files available via `CALDB`. The `nupipeline` version 0.4.9 was used to produce the clean event files. The `nuproduct` command was used to extract the light curves and spectrum corresponding to the source and background regions. A circle of radius 90 arcsec around the source position was used for extracting the source level 2 products. Similarly, a circle of the same radius away from the source region was used to extract the background products. Barycenter correction was performed using `barycorr` v2.16. All the spectral files were optimally binned based on Kaastra and Bleeker (2016).

For the joint fitting with the spectra from the two modules of FPM, the normalization factor of one of the modules (FPMA) was fixed to unity while the other (FPMB) factor was left to vary. All the spectral analysis was carried out using XSPEC version 12.12.1 (Arnaud, 1996) with the absorption by interstellar medium modeled using the Tuebingen–Boulder absorption model `TBabs` and abundance taken from Wilms et al. (2000) and the photoelectric cross sections from Verner et al. (1996).

3. Data analysis

3.1. Timing analysis

The light curve from *Cep X-4* shows significant variations in count rate between the two observations. The count rate of the source changed from 0.28 counts/s for ObsID 02 to 0.074 counts/s for ObsID 04. *Cep X-4* is known to exhibit pulsation with a period of ∼ 66 s Using the epoch folding (Leahy, 1987) tool `efsearch`, we determined the spin period of the NS during the first observation to be 66.38 (1) s. The folded pulse profile for *Cep X-4* in the entire *NuSTAR* energy range of 3–79 keV is plotted in the top panel of Fig. 2. The pulse profile is single-peaked in nature, with complex sub-pulse features. During the second observation, the pulsations were detected with the same period of 66.38 (1) s. The overall profile, as seen in red in Fig. 2, remains similar to ObsID 02.

The pulse fraction (PF) for a pulse profile (P) can be defined as

$$PF = \frac{P(max) - P(min)}{P(max) + P(min)} \quad (2)$$

where P(max) and P(min) are the maximum and minimum of the pulse profile. The pulse fraction of *Cep X-4* in the broad energy band of 3–79 keV was calculated to be 64 ± 9 % for ObsID 02 and for 49 ± 15 % ObsID 04. To study the variation of pulse profile with energy, we extracted source light curves in the energy ranges of 3–5, 5–10, 10–20, 20–35 and 35–79 keV for both observations. The energy resolved profiles are plotted in Fig. 2 in black for ObsID 02 and in red for ObsID 04. There

was no significant detection of pulsations from the source in the 35–79 keV energy range during this period. The overall pulse profile remains very consistent across the two observations, with minor changes in the sub-pulse shape. The pulse fraction is found to be increasing with energy for both observations.

3.2. Spectral analysis

The broadband spectra of highly magnetized accreting X-ray pulsars are usually modeled using the powerlaw model with an exponential cutoff at higher energies (Coburn et al., 2002, and references therein). We have tried modeling the spectra with a powerlaw continuum with multiple cutoff models like `highECut`, `FDcut` (Tanaka, 1986), and `NewHCut` (Burderi et al., 2000) as well as physically motivated models like `CompST` (Sunyaev and Titarchuk, 1980) and `NPEX` (Makishima et al., 1999). The `NPEX` continuum model was finally chosen as it yields the lowest χ^2 in the fitting. The *Negative and Positive power law with a common EXponential cutoff factor*, i.e. `NPEX` model given by Eq. (3) describes unsaturated Comptonized emission.

$$\mathrm{NPEX}(E) = A(E^{-\Gamma} + f \times E^2)e^{-E/\beta} \tag{3}$$

The best-fit parameters for the spectral modeling are given in Table 2 with errors provided at a 90% confidence interval. Due to the lack of low energy coverage from *NuSTAR*, the absorption column density was fixed at a value of 0.8×10^{22} atoms cm^{-2}, which corresponds to the Galactic absorption component along the line of sight (Kalberla et al., 2005; HI4P.I. Collaboration et al., 2016). The power law index of the `NPEX` model was $1.3^{+0.1}_{-0.1}$, which is much softer than previously observed (Bhargava et al., 2019). The exponential cutoff value of $6.4^{+0.5}_{-0.4}$ keV is consistent with older observations of the source (Makishima et al., 1999). The residual from the spectral fitting with the `NPEX` showed spectral residuals near 30 keV, where a cyclotron line is known to be present in the source (Mihara et al., 1991). Hence, an additional absorption component was used to model the cyclotron absorption feature. The addition of the cyclotron line gave a $\Delta\chi^2$ of 24 for 3 additional d.o.f. The central energy of the CRSF was found at $27.3^{+1.5}_{-1.0}$ keV with a width of $2.2^{+1.1}_{-1.0}$ keV and an optical depth of $0.83^{+0.43}_{-0.31}$. The final spectral model used to describe the continuum was *tbabs* × *NPEX* × *gabs*. The presence of the cyclotron line was also observed with the other spectral models with the CRSF parameters similar to the values given in Table 2. The best fit spectral model, along with individual components, are plotted in Fig. 3. Allowing the absorption column density to vary gave a higher value of NH of about 8×10^{22} cm^{-2} and a softer powerlaw index. Other parameters obtained were consistent within the error.

The significance of the CRSF feature was calculated by making 100,000 simulations of the data using the *XSPEC* tool `simftest`. In each of the simulations, spectral models were fitted with and without the absorption feature and the corresponding best-fit χ^2 values were calculated. The false-detection probability was then calculated to be about 0.06%, making the detection significant at a confidence interval of 3.4 σ. During this observation, the unabsorbed source flux was calculated to be $2.0^{+0.1}_{-0.1} \times 10^{-11}$ erg s^{-1} cm^{-2} in the 3–79 keV energy range. Assuming a distance of 7.4 kpc, the luminosity of the source during this observation was calculated to be $1.3^{+0.1}_{-0.1} \times 10^{35}$ erg s^{-1}.

During the second observation, ObsID 04, the source count rate was lower by a factor of ∼5 with respect to ObsID 02. The spectra for ObsID 04 can be well described with an absorbed `NPEX` model *tbabs* × *NPEX*. Similar to the first observation the absorption column density was frozen to the Galactic line of sight value. The best-fit power law index was 1.7 ± 0.3, similar to the power law index for the source during ObsID 02. The best-fit spectral model for ObsID 04 is shown in Fig. 4. The unabsorbed flux from the source was calculated to be $4.4^{+0.4}_{-0.4} \times 10^{-12}$ erg cm^{-2} s^{-1} in the 3–79 keV energy range. The luminosity of the source was calculated to be $3.0^{+0.2}_{-0.2} \times 10^{34}$ erg s^{-1}, assuming a distance of 7.4 kpc. The best fit spectral parameters with the errors quoted for 90% confidence interval are given in Table 2. With prior knowledge of the presence of CRSF in *Cep X-4*, we looked for a cyclotron line in the spectrum during ObsID 04. Since the line energy and width could not be constrained, it was frozen to the value obtained from ObsID 02. The optical depth of the line had an upper limit of 1.7, with no significant improvement of χ^2 with the addition of the new spectral component. The CRSF has a false detection probability of 28%, making the CRSF detection in ObsID 04 not significant.

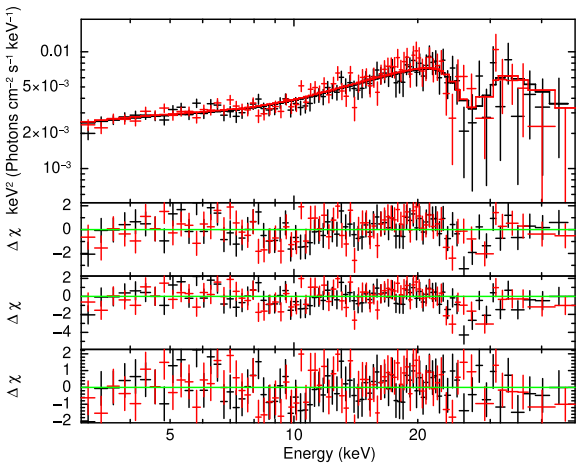

Fig. 3. Spectrum and best-fit spectral model for ObsID 02. The top panel correspond to the best-fit model along with the different components. The second panel from top panel shows the residual from the best fit model without adding the CRSF. While the third panel from top shows the residual obtained by setting the strength of the CRSF to zero. The bottom panel corresponds to the best-fit model residuals. The black points correspond to FPMA, while the red points are for FPMB.

Table 2
The table contains the best-fit spectral parameters of the *Cep X-4*for both observations. The errors are quoted at 90% confidence intervals.

Spectral parameter	ObsID 02	ObsID 04
N_H [$\times 10^{22}$ cm^{-2}]	0.8 (frozen)	0.8 (frozen)
Photon Index (Γ)	$1.3^{+0.1}_{-0.1}$	$1.7^{-0.3}_{+0.3}$
f_{NPEX} [10^{-4}]	$4.6^{+1.0}_{-0.8}$	$4.2^{+2.0}_{-1.3}$
β_{NPEX} (keV)	$6.4^{+0.5}_{-0.4}$	$5.2^{+0.7}_{-0.5}$
Norm_{NPEX} {[}$\times 10^{-3}${]}	$1.9^{+0.3}_{-0.3}$	$1.2^{-0.5}_{+0.8}$
E_{CRSF} (keV)	$27.3^{+1.5}_{-1.0}$	–
σ_{CRSF} (keV)	$2.2^{+1.1}_{-1.0}$	–
τ_{CRSF} (keV)	$0.83^{+0.43}_{-0.31}$	–
Unabsorbed Flux[a]	$2.0^{+0.1}_{-0.1} \times 10^{-11}$	$4.4^{+0.4}_{-0.4} \times 10^{-12}$
Luminosity[b]	$1.3^{+0.1}_{-0.1} \times 10^{35}$	$3.0^{+0.2}_{-0.2} \times 10^{34}$
χ^2 (d.o.f.)	145.01 (154)	51 (37)

[a] The unabsorbed flux is given in the energy range of 3–79 keV in units of erg cm^{-2} s^{-1}.
[b] The luminosity is given in the energy range of 3–79 keV in units of erg s^{-1}.

4. Discussion

In this work, we report the results from the two *NuSTAR* observations of the transient BeXRP *Cep X-4* during its 2023 outburst. The two *NuSTAR* observations were carried out during the decay phase of the outburst. The broadband continuum spectra of *Cep X-4* were modeled using an absorbed `NPEX` model for both observations. The spectrum of *Cep X-4* became softer in ObsID 04 with respect to ObsID 02, with the decay of the outburst. Sokolova-Lapa et al. (2023) analyzed the combined data from two observations during the 2023 outburst. The combined data showed a CRSF at ∼ 29 keV. However, combining multiple observations with different powerlaw index, at different flux

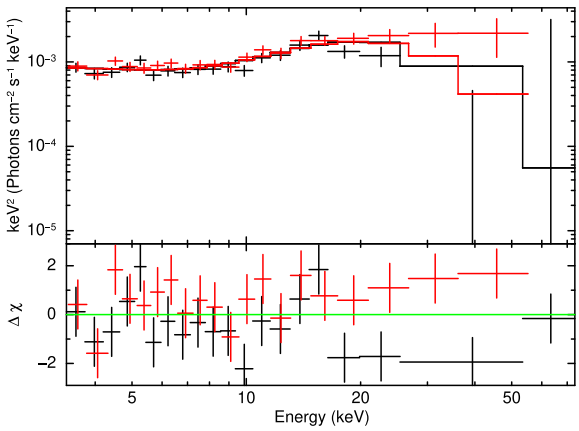

Fig. 4. Spectrum and best-fit spectral model for ObsID 04. The top panel correspond to the best-fit model. While the bottom panel corresponds to the best-fit model residuals. The black points correspond to FPMA, while the red points are for FPMB.

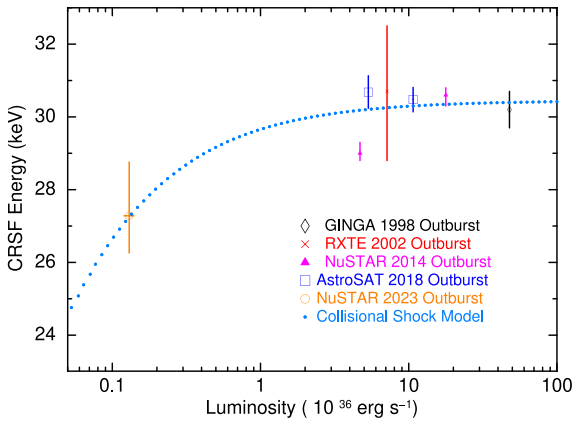

Fig. 5. The variation of cyclotron line energy with luminosity is plotted in the figure. The results from the collisionless shock plasma model are shown via the dotted line.

levels can lead to spurious features in the spectrum. A significantly high black body temperature (∼ 5 keV) was detected along with a broad Gaussian-like feature at ∼ 20 keV. The large blackbody component, along with the broad emission feature at about 20 keV, may be indicative of spurious spectral features from combining data across multiple flux ranges. A similar broad emission feature was observed in the *RXTE* data around ∼ 14 keV (McBride et al., 2007). A '10 keV feature' has been observed in many sources (Manikantan et al., 2023). An absorption feature was detected in the source in a similar energy range in *NuSTAR* data (Fürst et al., 2015; Vybornov et al., 2017), however, it was not identified as a '10 keV feature' (Manikantan et al., 2023). It is important to analyze the two observations separately so that the true spectral shape and their evolution can be properly studied. The source luminosity dropped by a factor of 4–5 between the two observations. The onset of propeller regime can be calculated using the formula

$$L_{prop} = 4 \times 10^{37}\ \xi^{7/2}\ B_{12}^{2}\ P^{-7/3}\ M_{1.4}^{-2/3}\ R_{6}^{5}\ \text{erg s}^{-1} \quad (4)$$

where B_{12} is the magnetic field strength in the unit of 10^{12} G, $M_{1.4}$ is the mass of the NS in units of 1.4 solar mass, R_6 is the radius of the NS in units of 10^6 cm, P is the spin period of the NS in s and ξ is the factor that relates the magnetospheric radius for disc accretion to the Alfven radius calculated assuming spherical accretion (Campana et al., 2002). We assume the mass and radius of the NS to be the canonical value of 1.4 solar mass and 10^6 cm respectively. The value of ξ is usually assumed to be 0.5 (Ghosh and Lamb, 1978). The onset of propeller regime was calculated from Eq. (4) to be 7.3 $\times 10^{33}$ erg s^{-1} which is less than the luminosity corresponding to the two *NuSTAR* observations. Pulsations were also detected in the source during ObsID 04, therefore, the second *NuSTAR* observation was taken before the onset of propeller regime in *Cep X-4*.

A CRSF was detected in *Cep X-4* during ObsID 02 at around 27 keV. The spectral shape of X-ray pulsars at a low luminosity sometimes show double-humped shape, which may be interpreted as a 'cyclotron' feature (Sokolova-Lapa et al., 2021). However, the CRSF in *Cep X-4* was present for multiple continuum spectral models around ∼ 27 keV energy range, making it unlikely that the absorption feature is due to shape of the X-ray spectrum at low luminosity. The detection of the cyclotron line at low luminosity needs to be considered to update the luminosity dependence of the cyclotron line. The detection of CRSF at low luminosity has been greatly facilitated by the high effective area and good spectral resolution of the *NuSTAR* telescope.

4.1. Luminosity variation of CRSF

We combine the results from all previous detection of CRSF in *Cep X-4* along with the data from the two 2023 *NuSTAR* observations. The details of the archival CRSF measurements in *Cep X-4* (Mukerjee and Antia, 2021) are given in Table 3. The luminosity corresponding to each observation was calculated by taking the flux value from Table 3 and assuming a distance of 7.4 ± 0.5 kpc (Bailer-Jones et al., 2021; Gaia Collaboration et al., 2023). The CRSF central energy as a function of luminosity is plotted in Fig. 5. There seems to be a positive correlation between E_{cyc} and L_X with long-term data, unlike previously reported (Mukerjee and Antia, 2021). The CRSF energy saturates at higher luminosity, which can be misinterpreted as a constant CRSF line energy that does not vary with luminosity. The positive correlation is in agreement with similar results reported from pulse-amplitude resolved analysis (Vybornov et al., 2017).

4.2. Collisionless shock model

The persistent X-ray pulsar Her X-1 was the first source where a positive correlation between E_{cyc} and L_x was observed (Staubert et al., 2007). Subsequently, similar relationships were identified in a number of persistent and transient sources like A 0535+63 (Caballero et al., 2008; Müller et al., 2013), Swift J1626.6−5156 (DeCesar et al., 2013), Vela X-1 (Fürst et al., 2014; La Parola et al., 2016), GX 304−1 (Malacaria et al., 2015; Rothschild et al., 2017) and 2S 1553-542 (Malacaria et al., 2022). Recent reanalysis of the CRSF energy in 4U 0115+ 63 across multiple outbursts has also revealed a positive correlation between E_{cyc} and L_x across a wide range in luminosity (Roy et al., 2024).

In the collisionless shock regime, a positive correlation between cyclotron line energy and luminosity is expected (Becker et al., 2012). However, beyond a critical luminosity threshold, the CRSF energy and luminosity have a negative correlation (Staubert et al., 2019). The line center is a direct measure of the magnetic field strength at the CRSF forming region. In systems exhibiting a positive correlation, there is a decrease in the height of the CRSF forming region from the NS surface, with an increase in luminosity, leading to an increase in E_{cyc}. The collisionless shock model was used to explain the luminosity dependency of CRSF observed in Her X−1 (Staubert et al., 2007).

The height (H_S) of the collisionless shock forming region above the NS surface is inversely proportional to the electron density (n_e) as $H_S \propto 1/n_e$ (Shapiro and Salpeter, 1975). The electron density in the accretion column is a function of mass accretion rate ($\dot{M}$) and area of the accretion flow (A) on the NS surface as $n_e \propto \dot{M}/A$. The area of the accretion flow is inversely proportional to magnetospheric

Table 3
Cyclotron line energy measurements of *Cep X-4*.

Observation	Telescope	MJD	Source Flux[a] (erg cm^{-2} s^{-1})	CRSF$_{center}$ Energy (keV)	CRSF$_{width}$ Width (keV)	CRSF$_{op-depth}$ Depth (τ)	Ref.
1988 April	*GINGA*	47 264	7.23×10^{-9}[a]	$30.2^{+0.5}_{-0.5}$	$16.1^{+1.8}_{-1.8}$	$2.88^{+0.11}_{-0.11}$	[1]
2002 July	*RXTE*	52 451	1.08×10^{-9}[b]	$30.7^{+1.8}_{-1.9}$	$3.6^{+2.9}_{-1.5}$	$0.7^{+0.3}_{-0.2}$	[2]
2014 June	*NuSTAR*	56 827	2.69×10^{-9}	$30.6^{+0.2}_{-0.3}$	$3.9^{+0.2}_{-0.2}$	$6.6^{+0.9}_{-0.8}$[c]	[3]
2014 July		56 840	7.10×10^{-10}	$29.0^{+0.3}_{-0.2}$	$3.8^{+0.2}_{-0.2}$	$7.0^{+0.8}_{-0.6}$[c]	
2018 July	*AstroSat*	58 302	1.62×10^{-9}	$30.48^{+0.33}_{-0.34}$	$3.24^{+1.14}_{-0.93}$	$1.03^{+0.14}_{-0.11}$	[4]
2018 July		58 307	8.08×10^{-10}	$30.68^{+0.45}_{-0.44}$	$5.89^{+1.38}_{-1.26}$	$1.42^{+0.18}_{-0.18}$	
2023 July	*NuSTAR*	60 132	2.0×10^{-11}	$27.3^{+1.5}_{-1.0}$	$2.2^{+1.1}_{-1.0}$	$0.83^{+0.43}_{-0.31}$	[5]

References : [1] Mihara et al. (1991) [2] McBride et al. (2007) [3] Vybornov et al. (2017) [4] Mukerjee and Antia (2021) [5] Present Work.

[a] The source flux is calculated in the 3–78 keV range.

[b] Corrected flux in 3–78 keV energy band taken from Mukerjee & Antia (2021).

[c] Expressed in terms of absorption depth (d) related to optical depth $\tau = d/(\sqrt{2\pi}\sigma)$.

radius (R_m). The variation of the magnetospheric radius with mass accretion rate goes as $R_m \propto \dot{M}^{-x}$ where $x = 2/7$ for disc or Bondi quasi-spherical accretion (Shakura et al., 2012). Therefore, the shock forming height from the NS surface as a function of mass accretion rate can be expressed as,

$$H_s(\dot{M}) \propto \dot{M}^{\alpha} \tag{5}$$

where $\alpha = 1-x = 5/7$ for disc or Bondi quasi-spherical accretion, which is the case for *Cep X-4*. The height of collisionless shock decreases with an increase in the mass accretion rate, which moves the CRSF line forming region towards stronger magnetic field strength. In a dipolar magnetic field, strength varies with the distance (r) from the NS as $B(r) \propto 1/r^3$. Therefore the cyclotron line energy (E_{cyc}) as a function of mass accretion rate can be written as,

$$E_{cyc}(\dot{M}) = E_0 \left(\frac{R_{NS}}{H_s(\dot{M}) + R_{NS}}\right)^3 \left(\frac{z_s}{Z_H}\right) \tag{6}$$

where E_0 is the cyclotron line energy corresponding to the magnetic field strength near the magnetic poles on the NS surface (Rothschild et al., 2017; Roy et al., 2024). The mass accretion rate is directly proportional to the X-ray luminosity (L_X), so we can write the ratio of the shock forming height to the NS radius as

$$\frac{H_s(\dot{M})}{R_{NS}} = K L_X^{-\alpha} \tag{7}$$

where K is the proportional constant regulating the height of the shock-forming region. Combining equation (6) and (7), the CRSF line energy can be written as a function of X-ray luminosity as,

$$E_{cyc}(L_X) = E_0 \left(1 + \frac{K}{L_X^{\alpha}}\right)^{-3}. \tag{8}$$

where α is taken as 5/7 corresponding to disc accretion (Shakura et al., 2012).

The best-fit values of the two free parameters E_0 and K were calculated to be 30.45 ± 0.27 keV and 0.009 ± 0.002 (erg/s)$^{\alpha}$ respectively. The surface magnetic field strength and the proportionality constant was calculated to be 31.4 ± 0.2 and 0.024 ± 0.003 (erg/s)$^{\alpha}$ from pulse height resolved analysis (Vybornov et al., 2017). The model prediction for E_{cyc} as a function of luminosity L_X is plotted in blue in Fig. 5. The calculated value of the magnetic field close to the NS in this work is a little lower compared to the estimates by Vybornov et al. (2017). The estimated cyclotron line energy at the surface of the NS gives a magnetic field strength of 2.6×10^{12} G from Eq. (1).

The critical luminosity can be expressed as a function of NS parameters as

$$L_{crit} = 1.49\times10^{37} \left(\frac{\Lambda}{0.1}\right)^{-7/5} (\omega)^{-28/15} \left(\frac{R}{10^6 cm}\right)^{1/10} \left(\frac{M}{1.4M_{\odot}}\right)^{29/30} \left(\frac{B}{10^{12}G}\right)^{16/15} erg/s \tag{9}$$

where ω depends on the shape of the spectrum and Λ accounts for particular uncertainties in the magnetospheric radius effects (Becker et al., 2012). Following (Becker et al., 2012) we take the value of Λ to be 0.1 and ω as 1. Assuming canonical values of NS mass to be 1.4 $M_{\odot}$, NS radius of 10 km, and surface magnetic field strength of 2.6×10^{12} G, the critical luminosity can be calculated as 4×10^{37} erg/s. The Coulombic luminosity (L_{coul}) value based on formula given in Becker et al. (2012) was calculated for *Cep X-4* to be ~ 8.5 $\times10^{36}$ erg s^{-1}. The accretion onto the NS is expected to settle onto the NS surface at luminosities less than L_{coul}. The luminosity of *Cep X-4* in ObsID 04 is an order of magnitude lower than the L_{coul}. However, the calculation of L_{coul} is based on a simplistic picture of the accretion column and calculated with rough estimates of parameters based on simple assumptions. A different set of parameter values can give an order of magnitude lower estimate for L_{coul}. The 'critical' luminosity values based on exact value of Compton scattering cross section in high magnetic fields was calculated to be ~ 1.1 $\times10^{37}$ erg s^{-1} (Mushtukov et al., 2015) indicating that the second *NuSTAR* observation during the 2018 outburst and the *GINGA* data might have been taken in the 'super-critical' accretion regime. However, due to sparse observation above L_{crit}, it is harder to see any correlation and established the switch to negative correlation as predicted for super-critical regime. We consider all the data used in this analysis to be in the 'sub-critical' accretion regime where shock height is determined by Columbic interactions (Becker et al., 2012).

5. Summary and conclusions

The luminosity dependence of *Cep X-4* has evolved over subsequent high-sensitivity observations. Pulse amplitude resolve analysis during the 2014 outburst showed a positive correlation between CRSF energy and X-ray luminosity (Vybornov et al., 2017). However, using data across multiple outbursts, the CRSF line energy showed no variation with X-ray luminosity nor any evolution with time (Mukerjee and Antia, 2021). Using *NuSTAR* data from the most recent outburst, we showed that from long-term data also, there is a positive relation between CRSF energy and luminosity. The collisionless shock model well explains the observed variations between L_X and E_{cyc}. This gives us a surface magnetic field strength of 2.6×10^{12} G.

The results of surface magnetic field strength from long term (this work) and pulse-amplitude resolved analysis (Vybornov et al., 2017) are in agreement at 2σ level, however, the proportionality constant are much different as is expected for comparison between very different luminosity levels. We do not actually have a good physical model that explains X-ray emission from the NS accretion column across a wide range of X-ray luminosity (for detailed study refer to Sokolova-Lapa

et al., 2021 or D'Aì et al., 2025 and references therein). For persistent sources that do not show significant long-term variation in flux, a pulse amplitude resolved analysis can be used to estimate the magnetic field strength at the NS surface. This is particularly important for sources that have very limited observations with sensitive instruments like *NuSTAR*.

CRediT authorship contribution statement

Kinjal Roy: Writing – original draft, Resources, Investigation, Formal analysis. **Rahul Sharma:** Supervision.

Declaration of competing interest

The authors declare that they have no known competing financial interests or personal relationships that could have appeared to influence the work reported in this paper.

Acknowledgments

The authors thank the anonymous referee for their comments and suggestions which has helped to improve the quality of the paper. KR would like to thank Biswajit Paul, Ashwin Devaraj, and Ajith B. for their inputs during the preparation of the manuscript. This research made use of data obtained with *NuSTAR* a project led by Caltech, funded by NASA, United States and managed by NASA/JPL.

Data availability

Data will be made available on request.

References

Arnaud, K.A., 1996. XSPEC: The first ten years. In: Jacoby, G.H., Barnes, J. (Eds.), Astronomical Data Analysis Software and Systems V. In: Astronomical Society of the Pacific Conference Series, vol. 101, p. 17.

Bailer-Jones, C.A.L., Rybizki, J., Fouesneau, M., Demleitner, M., Andrae, R., 2021. Estimating distances from parallaxes. V. Geometric and photogeometric distances to 1.47 billion stars in gaia early data release 3. Astron. J. 161 (3), 147. http://dx.doi.org/10.3847/1538-3881/abd806, arXiv:2012.05220.

Becker, P.A., Klochkov, D., Schönherr, G., Nishimura, O., Ferrigno, C., Caballero, I., Kretschmar, P., Wolff, M.T., Wilms, J., Staubert, R., 2012. Spectral formation in accreting X-ray pulsars: bimodal variation of the cyclotron energy with luminosity. Astron. Astrophys. 544, A123. http://dx.doi.org/10.1051/0004-6361/201219065, arXiv:1205.5316.

Bhargava, Y., Bhalerao, V., Ballhausen, R., Fürst, F., Pottschmidt, K., Tomsick, J.A., Wilms, J., 2019. Explaining the asymmetric line profile in cepheus X-4 with spectral variation across pulse phase. Mon. Not. RAS 482 (3), 2902–2912. http://dx.doi.org/10.1093/mnras/sty2823, arXiv:1810.07724.

Burderi, L., Di Salvo, T., Robba, N.R., La Barbera, A., Guainazzi, M., 2000. The 0.1-100 KEV spectrum of centaurus X-3: Pulse phase spectroscopy of the cyclotron line and magnetic field structure. Astrophys. J. 530 (1), 429–440. http://dx.doi.org/10.1086/308336.

Caballero, I., Santangelo, A., Kretschmar, P., Staubert, R., Postnov, K., Klochkov, D., Camero-Arranz, A., Finger, M.H., Kreykenbohm, I., Pottschmidt, K., Rothschild, R.E., Suchy, S., Wilms, J., Wilson, C.A., 2008. The pre-outburst flare of the A 0535+26 august/september 2005 outburst. Astron. Astrophys. 480 (2), L17–L20. http://dx.doi.org/10.1051/0004-6361:20079310, arXiv:0801.3167.

Campana, S., Stella, L., Israel, G.L., Moretti, A., Parmar, A.N., Orlandini, M., 2002. The quiescent X-Ray emission of three transient X-Ray pulsars. Astrophys. J. 580 (1), 389–393. http://dx.doi.org/10.1086/343074, arXiv:astro-ph/0207422.

Coburn, W., Heindl, W.A., Rothschild, R.E., Gruber, D.E., Kreykenbohm, I., Wilms, J., Kretschmar, P., Staubert, R., 2002. Magnetic fields of accreting X-Ray pulsars with the Rossi X-Ray timing explorer. Astrophys. J. 580 (1), 394–412. http://dx.doi.org/10.1086/343033, arXiv:astro-ph/0207325.

D'Aì, A., Maniadakis, D.K., Ferrigno, C., Ambrosi, E., Sokolova-Lapa, E., Cusumano, G., Becker, P.A., Burderi, L., Del Santo, M., Di Salvo, T., Fürst, F., Iaria, R., Kretschmar, P., La Parola, V., Malacaria, C., Pinto, C., Pintore, F., Rodríguez-Castillo, G.A., 2025. Energy-resolved pulse profile changes in V 0332+53: Indications of wings in the cyclotron absorption line profile. Astron. Astrophys. 694, A316. http://dx.doi.org/10.1051/0004-6361/202451469, arXiv:2412.10907.

DeCesar, M.E., Boyd, P.T., Pottschmidt, K., Wilms, J., Suchy, S., Miller, M.C., 2013. The Be/X-Ray binary swift J1626.6-5156 as a variable cyclotron line source. Astrophys. J. 762 (1), 61. http://dx.doi.org/10.1088/0004-637X/762/1/61, arXiv:1211.3109.

Fürst, F., Pottschmidt, K., Miyasaka, H., Bhalerao, V., Bachetti, M., Boggs, S.E., Christensen, F.E., Craig, W.W., Grinberg, V., Hailey, C.J., Harrison, F.A., Kennea, J.A., Rahoui, F., Stern, D., Tendulkar, S.P., Tomsick, J.A., Walton, D.J., Wilms, J., Zhang, W.W., 2015. Distorted cyclotron line profile in cep X-4 as observed by NuSTAR. Astrophys. J. 806 (2), L24. http://dx.doi.org/10.1088/2041-8205/806/2/L24, arXiv:1505.02788.

Fürst, F., Pottschmidt, K., Wilms, J., Tomsick, J.A., Bachetti, M., Boggs, S.E., Christensen, F.E., Craig, W.W., Grefenstette, B.W., Hailey, C.J., Harrison, F., Madsen, K.K., Miller, J.M., Stern, D., Walton, D.J., Zhang, W., 2014. Nustar discovery of a luminosity dependent cyclotron line energy in Vela X-1. Astrophys. J. 780 (2), 133. http://dx.doi.org/10.1088/0004-637X/780/2/133, arXiv:1311.5514.

Gaia Collaboration, Vallenari, A., Brown, A.G.A., Prusti, T., de Bruijne, J.H.J., Arenou, F., Babusiaux, C., Biermann, M., Creevey, O.L., Ducourant, C., Evans, D.W., Eyer, L., Guerra, R., Hutton, A., Jordi, C., Klioner, S.A., Lammers, U.L., Lindegren, L., Luri, X., Mignard, F., Panem, C., Pourbaix, D., Randich, S., Sartoretti, P., Soubiran, C., Tanga, P., Walton, N.A., Bailer-Jones, C.A.L., Bastian, U., Drimmel, R., Jansen, F., Katz, D., Lattanzi, M.G., van Leeuwen, F., Bakker, J., Cacciari, C., Castañeda, J., De Angeli, F., Fabricius, C., Fouesneau, M., Frémat, Y., Galluccio, L., Guerrier, A., Heiter, U., Masana, E., Messineo, R., Mowlavi, N., Nicolas, C., Nienartowicz, K., Pailler, F., Panuzzo, P., Riclet, F., Roux, W., Seabroke, G.M., Sordo, R., Thévenin, F., Gracia-Abril, G., Portell, J., Teyssier, D., Altmann, M., Andrae, R., Audard, M., Bellas-Velidis, I., Benson, K., Berthier, J., Blomme, R., Burgess, P.W., Busonero, D., Busso, G., Cánovas, H., Carry, B., Cellino, A., Cheek, N., Clementini, G., Damerdji, Y., Davidson, M., de Teodoro, P., Nuñez Campos, M., Delchambre, L., Dell'Oro, A., Esquej, P., Fernández-Hernández, J., Fraile, E., Garabato, D., García-Lario, P., Gosset, E., Haigron, R., Halbwachs, J.L., Hambly, N.C., Harrison, D.L., Hernández, J., Hestroffer, D., Hodgkin, S.T., Holl, B., Janßen, K., Jevardat de Fombelle, G., Jordan, S., Krone-Martins, A., Lanzafame, A.C., Löffler, W., Marchal, O., Marrese, P.M., Moitinho, A., Muinonen, K., Osborne, P., Pancino, E., Pauwels, T., Recio-Blanco, A., Reylé, C., Riello, M., Rimoldini, L., Roegiers, T., Rybizki, J., Sarro, L.M., Siopis, C., Smith, M., Sozzetti, A., Utrilla, E., van Leeuwen, M., Abbas, U., Ábrahám, P., Abreu Aramburu, A., Aerts, C., Aguado, J.J., Ajaj, M., Aldea-Montero, F., Altavilla, G., Álvarez, M.A., Alves, J., Anders, F., Anderson, R.I., Anglada Varela, E., Antoja, T., Baines, D., Baker, S.G., Balaguer-Núñez, L., Balbinot, E., Balog, Z., Barache, C., Barbato, D., Barros, M., Barstow, M.A., Bartolomé, S., Bassilana, J.L., Bauchet, N., Becciani, U., Bellazzini, M., Berihuete, A., Bernet, M., Bertone, S., Bianchi, L., Binnenfeld, A., Blanco-Cuaresma, S., Blazere, A., Boch, T., Bombrun, A., Bossini, D., Bouquillon, S., Bragaglia, A., Bramante, L., Breedt, E., Bressan, A., Brouillet, N., Brugaletta, E., Bucciarelli, B., Burlacu, A., Butkevich, A.G., Buzzi, R., Caffau, E., Cancelliere, R., Cantat-Gaudin, T., Carballo, R., Carlucci, T., Carnerero, M.I., Carrasco, J.M., Casamiquela, L., Castellani, M., Castro-Ginard, A., Chaoul, L., Charlot, P., Chemin, L., Chiaramida, V., Chiavassa, A., Chornay, N., Comoretto, G., Contursi, G., Cooper, W.J., Cornez, T., Cowell, S., Crifo, F., Cropper, M., Crosta, M., Crowley, C., Dafonte, C., Dapergolas, A., David, M., David, P., de Laverny, P., De Luise, F., De March, R., 2023. Gaia data release 3. Summary of the content and survey properties. Astron. Astrophys. 674, A1. http://dx.doi.org/10.1051/0004-6361/202243940, arXiv:2208.00211.

Ghosh, P., Lamb, F.K., 1978. Disk accretion by magnetic neutron stars. Astrophys. J. 223, L83–L87. http://dx.doi.org/10.1086/182734.

Harrison, F.A., Craig, W.W., Christensen, F.E., Hailey, C.J., Zhang, W.W., Boggs, S.E., Stern, D., Cook, W.R., Forster, K., Giommi, P., Grefenstette, B.W., Kim, Y., Kitaguchi, T., Koglin, J.E., Madsen, K.K., Mao, P.H., Miyasaka, H., Mori, K., Perri, M., Pivovaroff, M.J., Puccetti, S., Rana, V.R., Westergaard, N.J., Willis, J., Zoglauer, A., An, H., Bachetti, M., Barrière, N.M., Bellm, E.C., Bhalerao, V., Brejnholt, N.F., Fuerst, F., Liebe, C.C., Markwardt, C.B., Nynka, M., Vogel, J.K., Walton, D.J., Wik, D.R., Alexander, D.M., Cominsky, L.R., Hornschemeier, A.E., Hornstrup, A., Kaspi, V.M., Madejski, G.M., Matt, G., Molendi, S., Smith, D.M., Tomsick, J.A., Ajello, M., Ballantyne, D.R., Baloković, M., Barret, D., Bauer, F.E., Blandford, R.D., Brandt, W.N., Brenneman, L.W., Chiang, J., Chakrabarty, D., Chenevez, J., Comastri, A., Dufour, F., Elvis, M., Fabian, A.C., Farrah, D., Fryer, C.L., Gotthelf, E.V., Grindlay, J.E., Helfand, D.J., Krivonos, R., Meier, D.L., Miller, J.M., Natalucci, L., Ogle, P., Ofek, E.O., Ptak, A., Reynolds, S.P., Rigby, J.R., Tagliaferri, G., Thorsett, S.E., Treister, E., Urry, C.M., 2013. The nuclear spectroscopic telescope array (NuSTAR) high-energy X-Ray mission. Astrophys. J. 770 (2), 103. http://dx.doi.org/10.1088/0004-637X/770/2/103, arXiv:1301.7307.

HI4P.I. Collaboration, Ben Bekhti, N., Flöer, L., Keller, R., Kerp, J., Lenz, D., Winkel, B., Bailin, J., Calabretta, M.R., Dedes, L., Ford, H.A., Gibson, B.K., Haud, U., Janowiecki, S., Kalberla, P.M.W., Lockman, F.J., McClure-Griffiths, N.M., Murphy, T., Nakanishi, H., Pisano, D.J., Staveley-Smith, L., 2016. HI4PI: A full-sky H I survey based on EBHIS and GASS. Astron. Astrophys. 594, A116. http://dx.doi.org/10.1051/0004-6361/201629178, arXiv:1610.06175.

Kaastra, J.S., Bleeker, J.A.M., 2016. Optimal binning of X-ray spectra and response matrix design. Astron. Astrophys. 587, A151. http://dx.doi.org/10.1051/0004-6361/201527395, arXiv:1601.05309.

Kalberla, P.M.W., Burton, W.B., Hartmann, D., Arnal, E.M., Bajaja, E., Morras, R., Pöppel, W.G.L., 2005. The Leiden/Argentine/Bonn (LAB) survey of galactic HI.

Final data release of the combined LDS and IAR surveys with improved stray-radiation corrections. Astron. Astrophys. 440 (2), 775–782. http://dx.doi.org/10.1051/0004-6361:20041864, arXiv:astro-ph/0504140.

Koyama, K., Kawada, M., Tawara, Y., Kimura, K., Kitamoto, S., Miyamoto, S., Tsunemi, H., Ebisawa, K., Nagase, F., 1991. A new X-Ray pulsar GS 2138+56 (cepheus X-4). Astrophys. J. 366, L19. http://dx.doi.org/10.1086/185900.

La Parola, V., Cusumano, G., Segreto, A., D'Aì, A., 2016. The swift-BAT monitoring reveals a long-term decay of the cyclotron line energy in Vela X-1. Mon. Not. RAS 463 (1), 185–190. http://dx.doi.org/10.1093/mnras/stw1915, arXiv:1608.06429.

Leahy, D.A., 1987. Searches for pulsed emission - improved determination of period and amplitude from epoch folding for sinusoidal signals. Astron. Astrophys. 180 (1–2), 275–277.

Makino, F., GINGA Team, 1988. X-Ray outburst. IAU Cirulars 4575, 1.

Makishima, K., Mihara, T., Nagase, F., Tanaka, Y., 1999. Cyclotron resonance effects in two binary X-Ray pulsars and the evolution of neutron star magnetic fields. Astrophys. J. 525 (2), 978–994. http://dx.doi.org/10.1086/307912.

Malacaria, C., Bhargava, Y., Coley, J.B., Ducci, L., Pradhan, P., Ballhausen, R., Fuerst, F., Islam, N., Jaisawal, G.K., Jenke, P., Kretschmar, P., Kreykenbohm, I., Pottschmidt, K., Sokolova-Lapa, E., Staubert, R., Wilms, J., Wilson-Hodge, C.A., Wolff, M.T., 2022. Accreting on the edge: A luminosity-dependent cyclotron line in the Be/X-Ray binary 2S 1553-542 accompanied by accretion regimes transition. Astrophys. J. 927 (2), 194. http://dx.doi.org/10.3847/1538-4357/ac524f, arXiv:2201.11376.

Malacaria, C., Klochkov, D., Santangelo, A., Staubert, R., 2015. Luminosity-dependent spectral and timing properties of the accreting pulsar GX 304-1 measured with INTEGRAL. Astron. Astrophys. 581, A121. http://dx.doi.org/10.1051/0004-6361/201526417, arXiv:1507.00595.

Manikantan, H., Paul, B., Rana, V., 2023. An investigation of the '10 keV feature' in the spectra of accretion powered X-ray pulsars with NuSTAR. Mon. Not. RAS 526 (1), 1–28. http://dx.doi.org/10.1093/mnras/stad2527, arXiv:2308.15129.

McBride, V.A., Wilms, J., Kreykenbohm, I., Coe, M.J., Rothschild, R.E., Kretschmar, P., Pottschmidt, K., Fisher, J., Hamson, T., 2007. On the cyclotron line in Cepheus X-4. Astron. Astrophys. 470 (3), 1065–1070. http://dx.doi.org/10.1051/0004-6361:20077238, arXiv:0705.2962.

Meszaros, P., 1992. High-energy radiation from magnetized neutron stars.

Mihara, T., Makishima, K., Kamijo, S., Ohashi, T., Nagase, F., Tanaka, Y., Koyama, K., 1991. Discovery of a cyclotron resonance feature at 30 keV from the transient X-Ray pulsar cepheus X-4. Astrophys. J. 379, L61. http://dx.doi.org/10.1086/186154.

Mukerjee, K., Antia, H.M., 2021. Studies of cepheus X-4 during the 2018 outburst observed with AstroSat. Astrophys. J. 920 (2), 139. http://dx.doi.org/10.3847/1538-4357/ac11f1, arXiv:2107.03608.

Müller, D., Klochkov, D., Caballero, I., Santangelo, A., 2013. A 0535+26 in the april 2010 outburst: probing the accretion regime at work. Astron. Astrophys. 552, A81. http://dx.doi.org/10.1051/0004-6361/201220347, arXiv:1303.6068.

Mushtukov, A.A., Suleimanov, V.F., Tsygankov, S.S., Poutanen, J., 2015. The critical accretion luminosity for magnetized neutron stars. Mon. Not. RAS 447 (2), 1847–1856. http://dx.doi.org/10.1093/mnras/stu2484, arXiv:1409.6457.

Nakajima, M., Niida, Y., Mihara, T., Negoro, H., Kobayashi, K., Tanaka, M., Soejima, Y., Kudo, Y., Kawamuro, T., Yamada, S., Tamagawa, T., Kawai, N., Matsuoka, M., Sakamoto, T., Serino, M., Sugita, S., Hiramatsu, H., Nishikawa, H., Yoshida, A., Tsuboi, Y., Urabe, S., Nawa, S., Nemoto, N., Shidatsu, M., Takahashi, I., Niwano, M., Sato, S., Higuchi, N., Yatsu, Y., Nakahira, S., Ueno, S., Tomida, H., Ishikawa, M., Ogawa, S., Kurihara, T., Ueda, Y., Setoguchi, K., Yoshitake, T., Nakatani, Y., Yamauchi, M., Hagiwara, Y., Umeki, Y., Otsuki, Y., Yamaoka, K., Kawakubo, Y., Sugizaki, M., Iwakiri, W., 2023. MAXI/GSC detection of an X-ray outburst from the Be/X-ray binary pulsar Cep X-4 (Ginga 2138+56). Astronomer' s Telegr. 16088, 1.

Raman, G., Varun, Pradhan, P., Kennea, J., 2023. Quiet, but not silent: uncovering quiescent state properties of two transient high-mass X-ray binaries. Mon. Not. RAS 526 (3), 3262–3272. http://dx.doi.org/10.1093/mnras/stad2577, arXiv:2308.12498.

Roche, P., Green, L., Hoenig, M., 1997. Cepheus X-4. IAU Cirulars 6698, 2.

Rothschild, R.E., Kühnel, M., Pottschmidt, K., Hemphill, P., Postnov, K., Gornostaev, M., Shakura, N., Fürst, F., Wilms, J., Staubert, R., Klochkov, D., 2017. Discovery and modelling of a flattening of the positive cyclotron line/luminosity relation in GX 304-1 with RXTE. Mon. Not. RAS 466 (3), 2752–2779. http://dx.doi.org/10.1093/mnras/stw3222, arXiv:1610.08944.

Roy, K., Manikantan, H., Paul, B., 2024. Luminosity dependence of the multiple cyclotron lines in 4U 0115+63. Astron. Astrophys. 690, A50. http://dx.doi.org/10.1051/0004-6361/202450395, arXiv:2407.13869.

Shakura, N., Postnov, K., Kochetkova, A., Hjalmarsdotter, L., 2012. Theory of quasi-spherical accretion in X-ray pulsars. Mon. Not. RAS 420 (1), 216–236. http://dx.doi.org/10.1111/j.1365-2966.2011.20026.x, arXiv:1110.3701.

Shapiro, S.L., Salpeter, E.E., 1975. Accretion onto neutron stars under adiabatic shock conditions. Astrophys. J. 198, 671–682. http://dx.doi.org/10.1086/153645.

Sokolova-Lapa, E., Gornostaev, M., Wilms, J., Ballhausen, R., Falkner, S., Postnov, K., Thalhammer, P., Fürst, F., García, J.A., Shakura, N., Becker, P.A., Wolff, M.T., Pottschmidt, K., Härer, L., Malacaria, C., 2021. X-ray emission from magnetized neutron star atmospheres at low mass-accretion rates. I. Phase-averaged spectrum. Astron. Astrophys. 651, A12. http://dx.doi.org/10.1051/0004-6361/202040228, arXiv:2104.06802.

Sokolova-Lapa, E., Zalot, N., Stierhof, J., Zainab, A., Wilms, J., Ballhausen, R., Malacaria, C., Kretschmar, P., Escorial, A.R., Pottschmidt, K., Fuerst, F., Ferrigno, C., Pradhan, P., Coley, J.B., 2023. Low-luminosity accretion in Cep X-4 during the transition to quiescence observed by NuSTAR. Astronomer' s Telegr. 16171, 1.

Staubert, R., Shakura, N.I., Postnov, K., Wilms, J., Rothschild, R.E., Coburn, W., Rodina, L., Klochkov, D., 2007. Discovery of a flux-related change of the cyclotron line energy in Hercules X-1. Astron. Astrophys. 465 (2), L25–L28. http://dx.doi.org/10.1051/0004-6361:20077098, arXiv:astro-ph/0702490.

Staubert, R., Trümper, J., Kendziorra, E., Klochkov, D., Postnov, K., Kretschmar, P., Pottschmidt, K., Haberl, F., Rothschild, R.E., Santangelo, A., Wilms, J., Kreykenbohm, I., Fürst, F., 2019. Cyclotron lines in highly magnetized neutron stars. Astron. Astrophys. 622, A61. http://dx.doi.org/10.1051/0004-6361/201834479, arXiv:1812.03461.

Sunyaev, R.A., Titarchuk, L.G., 1980. Comptonization of X-Rays in plasma clouds - typical radiation spectra. Astron. Astrophys. 86, 121.

Tanaka, Y., 1986. Observations of compact X-Ray sources. In: Mihalas, D., Winkler, K.-H.A. (Eds.), In: IAU Colloq. 89: Radiation Hydrodynamics in Stars and Compact Objects, vol. 255, p. 198. http://dx.doi.org/10.1007/3-540-16764-1_12.

Tsygankov, S., Wijnands, R., Lutovinov, A., Degenaar, N., Poutanen, J., 2017. The X−ray properties of Be/X−ray pulsars in quiescence. Mon. Not. RAS 470 (1), 126–141. http://dx.doi.org/10.1093/mnras/stx1255, arXiv:1703.04634.

Ulmer, M.P., Baity, W.A., Wheaton, W.A., Peterson, L.E., 1973. New transient source, cepheus X-4, observed by OSO-7. Astrophys. J. 184, L117. http://dx.doi.org/10.1086/181302.

Verner, D.A., Ferland, G.J., Korista, K.T., Yakovlev, D.G., 1996. Atomic data for astrophysics. II. New analytic FITS for photoionization cross sections of atoms and ions. Astrophys. J. 465, 487. http://dx.doi.org/10.1086/177435, arXiv:astro-ph/9601009.

Vybornov, V., Klochkov, D., Gornostaev, M., Postnov, K., Sokolova-Lapa, E., Staubert, R., Pottschmidt, K., Santangelo, A., 2017. Luminosity-dependent changes of the cyclotron line energy and spectral hardness in Cepheus X-4. Astron. Astrophys. 601, A126. http://dx.doi.org/10.1051/0004-6361/201630275, arXiv:1702.06361.

Wilms, J., Allen, A., McCray, R., 2000. On the absorption of X-Rays in the interstellar medium. Astrophys. J. 542 (2), 914–924. http://dx.doi.org/10.1086/317016, arXiv:astro-ph/0008425.